International Journal of Applied Earth Observations and Geoinformation 102 (2021) 102393

Contents lists available at ScienceDirect

International Journal of Applied Earth Observations and Geoinformation

journal homepage: www.elsevier.com/locate/jag

# Leaf water content estimation using top-of-canopy airborne hyperspectral data

Rahul Raj [a,b,d,*], Jeffrey P. Walker [b], Vishal Vinod [c], Rohit Pingale [d], Balaji Naik [e], Adinarayana Jagarlapudi [d]

[a] IITB-Monash Research Academy, India
[b] Monash University, Melbourne, Australia
[c] Indian Institute of Science, Bengaluru, India
[d] Indian Institute of Technology Bombay, India
[e] Jayashankar Telangana State Agricultural University, India

ARTICLE INFO

*Keywords:*
Early-stage vegetation water stress
Pure-pixel narrowband water-sensitive vegetation indices
Drone-based hyperspectral imaging
Leaf water content

ABSTRACT

Remotely sensed estimation of leaf water content (LWC) using optical data at early crop growth stage is important for identification of water-stressed plants. However, its accurate estimation is currently a major challenge due to the coarse spatial and spectral resolution of the available optical data, and the atmospheric impact on satellite-based remotely sensed data. Moreover, during early growth stages the canopy coverage is low, increasing the effect of the bare soil background on low spatial resolution data. Consequently, broadband optical data is insensitive to overtone frequencies of O-H stretching bonds of water molecules. Accordingly, this research developed a new model for estimating LWC based on newly identified, pure-pixel, water sensitive indices from high spatial resolution hyperspectral data. A hand-held field spectroradiometer and drone-based hyperspectral imager were used to collect temporal high spectral resolution hyperspectral data (Range: 400–1000 nm; Bandwidth: ~2.1 nm) at leaf level, together with destructively sampled leaves to measure their LWC using the oven-drying method. The spectroradiometer data were used to explore the wavelengths sensitive to vibrational overtone frequencies of O-H bonds of water molecules present in leaves. A total of seven water-sensitive wavelengths were identified, and corresponding normalised indices created for use with pure pixel narrowband hyperspectral data from vegetation. Farm scale maps of LWC were then created using drone-based hyperspectral data, based on minimum and maximum values of the above indices and 'days after sowing' information, through a gradient boost machine (GBM) model. The early growth stage maps of LWC were able to distinguish between water-stressed and well-irrigated plots with an $R^2$ of 0.93 and RMSE of 1.6% (g/g).

## 1. Introduction

Water is one of the most important input parameters for any grain crop production (Gabriel et al., 2017) as irrigation management has a major control on plant growth (Gonzalez-Dugo et al., 2010). Accordingly, crop water stress increases the difference between attainable and actual yield, with the 'yield gap' minimized through optimized irrigation (Mueller et al., 2012). Water also helps nutrients from the soil to travel to various parts of the plant, and so even with adequate nutrients supplied to the soil, the crop may show nutritional deficiency if the crop is suffering from water stress (Wang and Xing, 2016). Thus, for optimal farm management, information about the spatio-temporal distribution of crop water content plays a crucial role.

One way to identify potentially water-stressed areas in the farm is through soil moisture mapping. However, remote sensing techniques are currently incapable of directly measuring soil moisture across the effective root zone (~30–50 cm) of grain crops (Etminan et al., 2020; Shen et al., 2020; Xu et al., 2016; Finn et al., 2011; Walker et al., 2004). Accordingly, leaf water content (LWC) was used in this research to identify the water stress in plants by using narrowband hyperspectral data. This was done on the basis that diffuse radiation reflected towards the remote sensor from the plants contains information about

* Corresponding author at: IITB-Monash Research Academy, Mumbai, Agro-informatics lab, CSRE, India.
*E-mail addresses:* Rahul.Rahulraj@monash.edu (R. Raj), Jeff.Walker@monash.edu (J.P. Walker), Vishalvinod@acm.org (V. Vinod), Rohitpingale103@iitb.ac.in (R. Pingale), Balajinaikbanoth789@gmail.com (B. Naik), Adi@csre.iitb.ac.in (A. Jagarlapudi).

https://doi.org/10.1016/j.jag.2021.102393
Received 12 March 2021; Received in revised form 18 May 2021; Accepted 8 June 2021

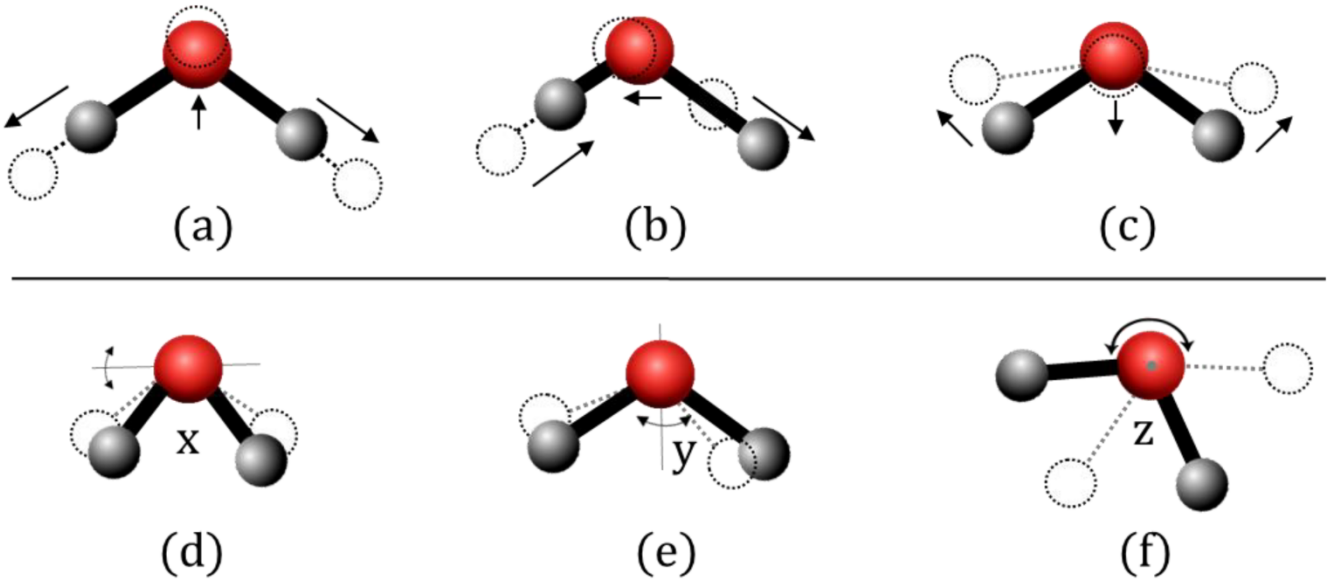


**Fig. 1.** (a), (b), and (c) shows the symmetric asymmetric, and bending stretch in water molecules. The red colour atom represents the oxygen (O) atom, and the grey colour atoms represent hydrogen (H) atoms. The arrows show the direction of motion of the atoms. (d), (e), and (f) show the three liberation modes of water molecules with respect to ×, y, and z axes (adapted from Chaplin, 2008). (For interpretation of the references to color in this figure legend, the reader is referred to the web version of this article.)

mesophyll's numerous air/cell interfaces of the leaves, which relate to the LWC of the plant (Vogelmann, 1993).

There are two different perspectives to plant water stress – instantaneous water stress and long-term water stress (Aroca, 2012). The effect of instantaneous water stress is a lowering of the LWC, which affects the gaseous exchanges between plants and their atmosphere (Ma et al., 2018). However, long-term water stress significantly affects crop biophysical parameters like Leaf Area Index, canopy height, and yield (Ma et al., 2018; Reddy et al., 2003; Blum, 2011; Pinheiro and Chaves, 2011). Thus instantaneous water stress in the crop that is not adequately managed creates the basis for long-term water stress, leading to a significant crop yield reduction (Hsiao et al., 1976). Conversely, the instantaneous water stress gives an early indication of potential yield loss (Ma et al., 2018), which can be avoided with correct ongoing irrigation management.

The LWC during early crop growth stage needs to be maintained above a critical value. For example, if the LWC of maize leaves goes below 82.5% (g/g) during the seedling/jointing stage, the photosynthetic rate may be reduced by as much as a factor of 3.2 (Ma et al., 2018). Moreover, the reduction in LWC below a critical level increases the loss in turgor pressure, further minimising the cell division and enhancement, resulting in inhibited leaf expansion and stomatal closure, which delays the gaseous exchanges between the plant and the atmosphere (Hsiao, 1973; Schulze and Hall, 1982; Blum, 2011; Pinheiro and Chaves, 2011). Thus, early detection of water-stressed plants by estimating LWC provides significant opportunities to ameliorate the stress through suitable agronomic management for improved crop yield.

Various sensors have been used for remote estimation of leaf (or vegetation) water content, including microwave (Huang et al., 2015; Hunt et al., 2011; Merlin et al., 2010; Yilmaz et al., 2008), thermal (Merlin et al., 2010; Yilmaz et al., 2008), and optical (Neinavaz et al., 2017; Gao et al., 2015; Ceccato et al., 2001; Clevers et al., 2010). However, microwave is low spatial resolution (Abowarda et al., 2021), thermal gets affected by the soil temperature especially when the canopy coverage is low (Han et al., 2016; Kim et al., 2016) and short-wave infrared are affected by the atmosphere (Thompson et al., 2019; Sicard et al., 1998). While the water absorption wavelengths above 1000 nm range (1940 nm, 1450 nm, and 1190 nm) have been the primary wavelengths for vegetation water sensing after atmospheric correction (Thenkabail and Lyon 2016), having stronger absorption of the electromagnetic spectrum than water absorption wavelengths between 400 and 1000 nm (Thenkabail and Lyon, 2016; Carter, 1991), sensors operating in this range are much more expensive and difficult to maintain. Importantly, a secondary water absorption band exists

**Table 1**
Water absorption bands in the visible and NIR region of the EM spectrum.

| EM region | Absorption Wavelength | Reason for absorption | Reference |
|---|---|---|---|
| VIS | 401 nm<br>449 nm | Fifth and sixth overtone of vibrational symmetric and asymmetric stretches of O—H bands | Pope and Fry, 1997<br>Stomp et al., 2007; Pope and Fry, 1997 |
| | 514/520 nm | Fifth overtone of vibrational symmetric and asymmetric stretches of O—H bands | Braun and Smirnov, 1993; Sogandares and Fry, 1997; Yakovenko et al., 2002; Stomp et al., 2007 |
| | 605 nm | Fourth overtone of vibrational symmetric and asymmetric stretches of O—H bands | |
| | 660 nm | Combined overtone of vibrational symmetric, asymmetric and bending stretches of O—H bands | Tsubomura et al., 1980; Braun and Smirnov, 1993 |
| | 698 nm | Fourth overtone of vibrational symmetric and asymmetric stretches of O—H bands | Braun and Smirnov, 1993 |
| IR | 750/760 nm | Small absorption peak due to third overtone of vibrational symmetric and asymmetric stretches of O—H bands | Tsubomura et al., 1980; Braun and Smirnov, 1993 |
| | 836/850 nm | Small absorption shoulder due to Combined overtone of vibrational symmetric, asymmetric, and bending stretches of O—H bands | |
| | 970/975 nm | Second overtone of vibrational symmetric, and asymmetric stretches of O—H bands | Tsubomura et al., 1980; Büning-Pfaue, 2003; Stomp et al., 2007 |

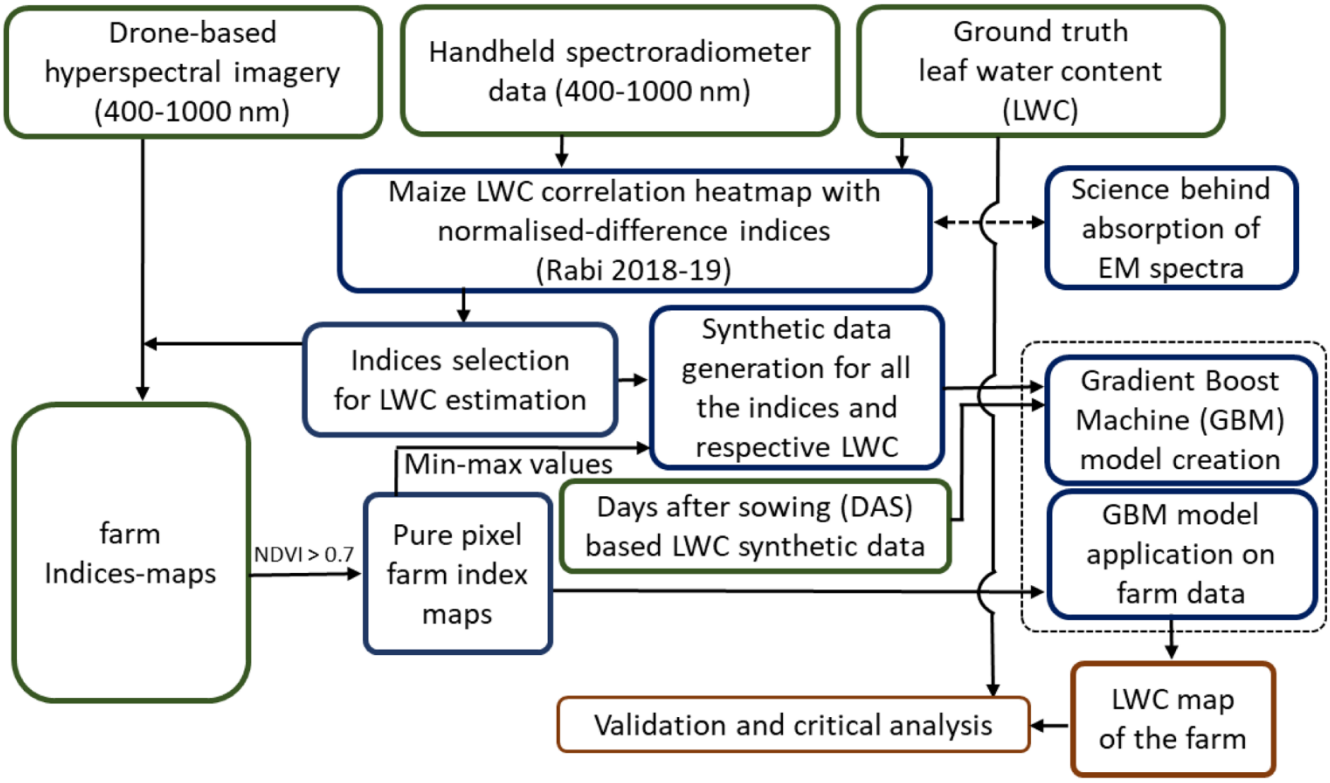


**Fig. 2.** The framework of the leaf water content (LWC) model development and evaluation.

between 400 and 1000 nm at around 970 nm (Thenkabail and Lyon 2016). Moreover, other wavelengths within the 400–1000 nm range also show sensitivity towards water molecules, but cannot offer any water content information in broadband and mixed pixel data. Accordingly, 400–1000 nm hyperspectral airborne data has been selected for the estimation of LWC here, being readily available at high resolution from UAV platforms.

Absorption of electromagnetic radiation by water molecules is determined by rotational transitions, intermolecular and intramolecular vibrational transitions, and electronic transitions of $H_2O$ molecules. Rotational transition and intermolecular vibrational transitions are responsible for absorption in the microwave and far-infrared electromagnetic (EM) spectrum region (Mohorič and Bren, 2020), with the electronic transitions creating absorption in the ultraviolet region (Underwood and Wittig, 2004). Absorption in the mid infrared (MIR) range is due to intramolecular vibrational transitions (Hunter et al., 2018), while in the VIS and NIR regions water absorption is majorly due to a stretching overtone frequency and vibrational absorption of the O-H bands of $H_2O$ molecules (Chaplin, 2008).

Water molecules vibrate in the symmetric stretch, asymmetric stretch, bend stretch and three liberation modes shown in Fig. 1 (Chaplin, 2008). Even though the VIS and NIR regions show very low water absorption characteristics compared to after 1000 nm, the water's overtone bands have been found to create spectral niches for photosynthetic organisms (Stomp et al., 2007). At 401 and 449 nm, water absorption can be seen due to the fifth and sixth overtone of vibrational

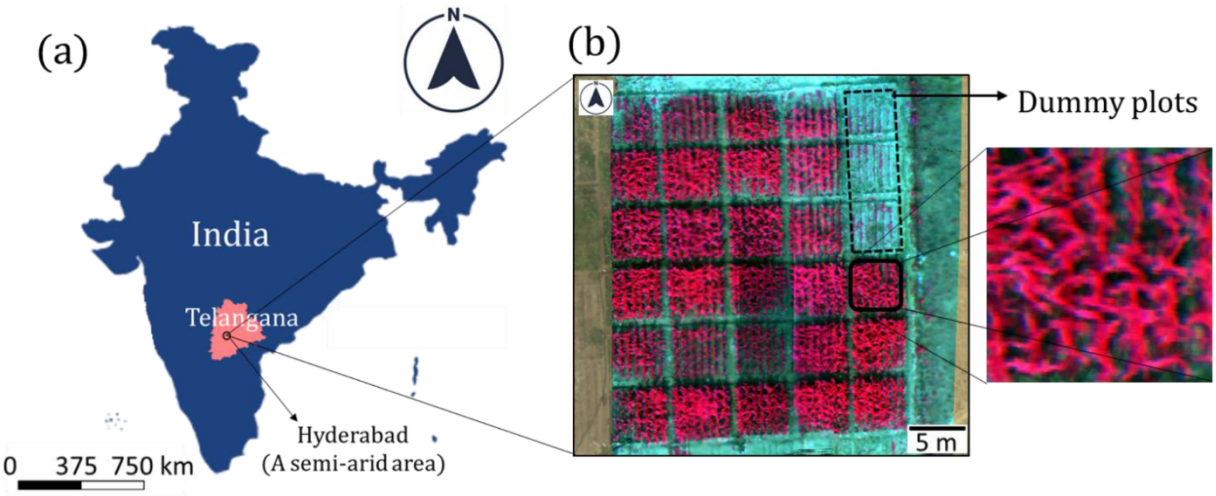


**Fig. 3.** (a) The geographical location of the farm that lies in the southern part of India and falls under a semi-arid zone. (b) The False-colour composite map of the research farm having leaf-level high-resolution hyperspectral data. Dummy plots shown are not part of research plots.

**Table 2**
Treatment information of the research farm for *Rabi* (Winter 2018–19). Here, CPE represents cumulative potential evaporation in mm, and IW means irrigated water in mm (50 mm for this research).

| Treatment | Meaning | Application rate |
|---|---|---|
| **N1** | High N stress | 100 kg/ha |
| **N2** | Ideal nitrogen | 200 kg/ha |
| **N3** | Overdose nitrogen | 300 kg/ha |
| **I1** | High water stress | Irrigation @ IW/CPE = 0.6 |
| **I2** | Moderate water stress | Irrigation @ IW/CPE = 0.8 |
| **I3** | No water stress | Irrigation @ IW/CPE = 1.2 |

symmetric, and asymmetric stretches of O—H bands (Pope and Fry, 1997; Stomp et al., 2007). It has also been found that the fifth overtone of the intramolecular stretches produces a very small absorption at 514 nm (Yakovenko et al., 2002; Sogandares and Fry, 1997; Braun and Smirnov, 1993; Stomp et al., 2007). At 605 nm, a fourth overtone band of symmetric and asymmetric stretches has been documented (Yakovenko et al., 2002; Sogandares and Fry, 1997; Braun and Smirnov, 1993; Stomp et al., 2007). At 660 nm, absorption occurs due to combined vibrational symmetric, asymmetric, and bending stretches of O-H overtone bonds (Tsubomura et al., 1980; Braun and Smirnov, 1993). At 698 nm, the fourth overtone of vibrational symmetric, and asymmetric stretches of the O-H bands has created water absorption in the EM spectrum (Braun and Smirnov, 1993). Spectroscopy has also shown a small absorption peak at 750 nm due to the third overtone of vibrational symmetric, and asymmetric stretches of O-H bands (Tsubomura et al., 1980; Braun and Smirnov, 1993). A water absorption shoulder has been observed at around 836–850 nm due to the combined overtone of vibrational symmetric, asymmetric, and bending stretches of O—H bands (Tsubomura et al., 1980; Braun and Smirnov, 1993). At 970 nm, water absorption band is found due to the second overtone of vibrational symmetric, and asymmetric stretches of O—H bands (Büning-Pfaue, 2003; Stomp et al., 2007). Table 1 shows the list of water absorption bands found from literature.

Most of the existing LWC estimation models available in hyperspectral sensing are based on mixed-pixel (vegetation and visible background in the same pixel) data taken either from satellite or high-altitude airborne platforms. These platforms can map huge areas but suffer from coarser spatial resolution (mixed-pixel) data that cannot capture the changes happening in the weak water-sensitive bands (Kokaly and Clark, 1999), especially when the crop is at the early growth stage with little canopy coverage (Cheng et al., 2006; Chen et al., 2005), due to the higher overtones of the water's O-H molecule stretching frequencies losing sensitivity for broadband and mixed pixel data (Thorpe et al., 2006; Thenkabail et al., 2002; Fan et al., 2009; Jones and Sirault, 2014). Moreover, optical observations from high altitude platforms are highly affected by atmospheric interference (aerosol, water vapour content, and various gases present in the atmosphere), which is incredibly challenging to correct due to limitations of 'atmospheric correction' algorithms (Gao et al., 2009; Zheng and Zeng, 2004). Accordingly, the small changes in these bands are unable to provide useful information on critical vegetation parameters from these sensors (Hadjimitsis et al., 2004).

Interestingly, Kim et al. (2010) used active hyperspectral sensing (whereby a consistent light source is used to illuminate the target to eliminate atmospheric effects) to identify the plant water stress on young apple trees and found narrowband 750 nm wavelength observations useful for LWC estimation. From Table 1, it can be seen that a small absorption peak exists at 750 nm due to the third overtone of vibrational symmetric and asymmetric stretches of O—H bonds. Moreover, Zygielbaum et al. (2009) has used 400–750 nm spectroradiometer data and found the 520 nm wavelength useful in the retrieval of relative water content from maize. In another study, Corti et al. (2017) has used the partial least square algorithm to estimate water stress in spinach plants using line-scanner camera-based 400–1000 nm hyperspectral data. However, Corti et al. (2017) could not point out specific bands related to water stress but gave ranges of wavelength based on the PLS algorithm. Feilhauer et al. (2015) have used PROSPECT model data along with leaf level spectroradiometer data (400–2500 nm) of various crops to select spectral bands for LWC ($g/cm^2$) estimation. Using an ensemble approach, bands near 750 nm were identified from the 400–1000 nm range for LWC estimation. From the 1000–2500 nm range, 1412 nm, 1978 nm, 2004 nm, and 2401 nm were identified for LWC estimation. While Casas et al. (2014) identified that the longer short-wave infrared region based indices gave improved correlation with canopy water content, this data is not readily available. Consequently, this paper has developed a new method for LWC estimation to identify the water-stressed areas of a farm at an early growth stage of the crop by using narrowband hyperspectral (400–1000 nm) drone-based high resolution

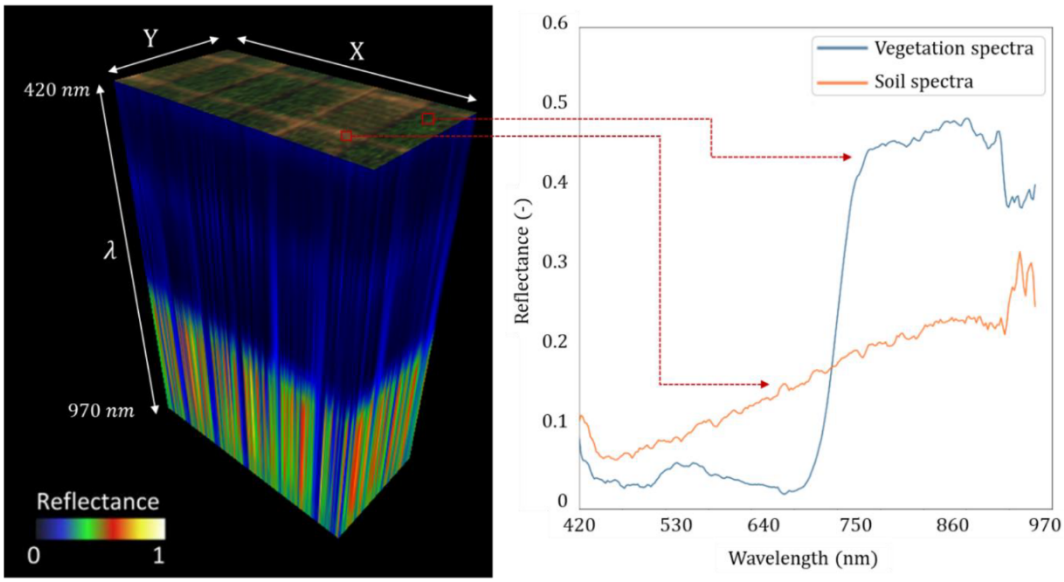


**Fig. 4.** Hyperspectral data cube - a three-dimensional representation of a hyperspectral image. Here, X and Y represent the spatial dimension while the Z dimension (denoted by$\lambda$) shows the spectral information according to wavelength for each pixel in the image. The top layer of the cube is showing an RGB map of a section of the farm. The spectral information of a vegetation and soil pixel is shown at the right of the plot.

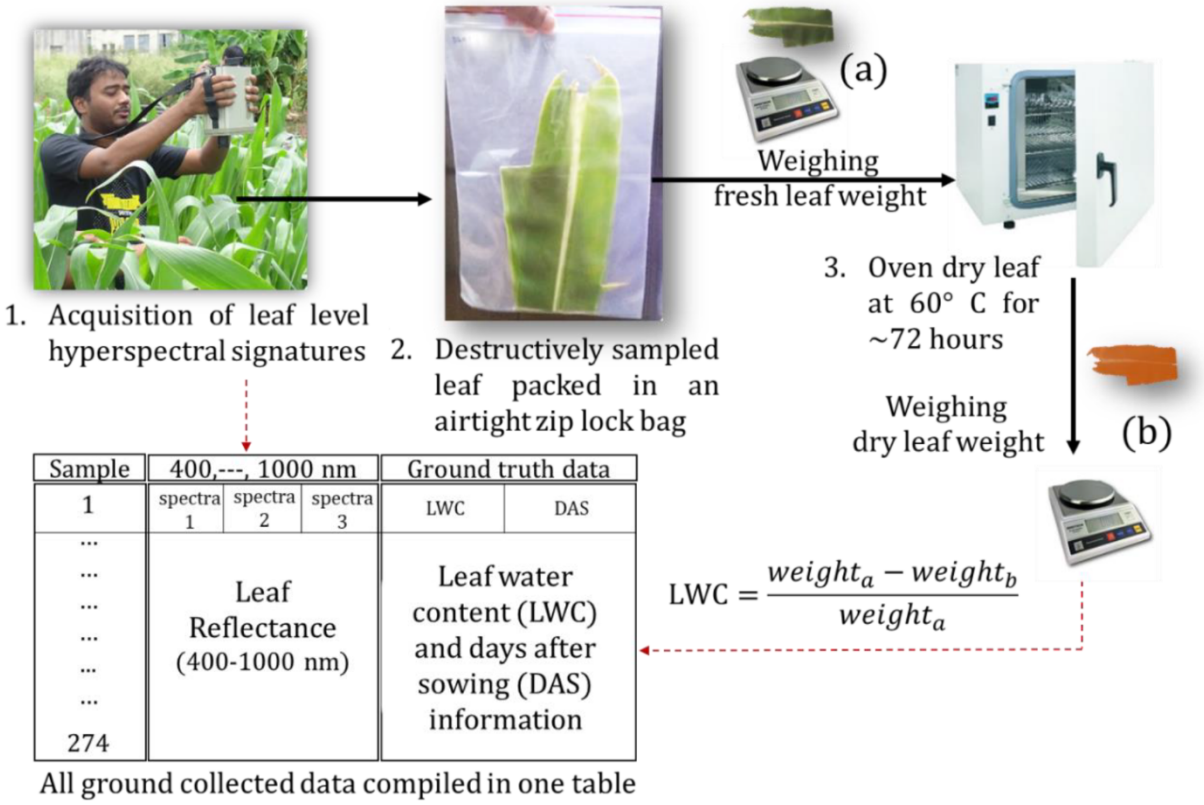


**Fig. 5.** Three leaf spectra per leaf of each subplot were collected using a hand-held spectroradiometer. The same leaves were destructively sampled, weighed, oven-dried, and leaf water content (LWC) calculated based on the difference between fresh and dry leaf weights. The obtained information about LWC was then saved with the respective leaf spectra along with days after sowing information for further data analysis.

data, thus overcoming the limitations of broadband, high altitude, low resolution data.

## 2. Materials and methods

In this study, a drone-based push-broom hyperspectral (400–1000 nm) imager was used to collect temporal data from a research farm. Hand-held spectroradiometer data was collected coincident with the flights to provide leaf-level spectral signatures (400–1000 nm) from plants grown in plots treated with different water and fertiliser doses. These leaves were subsequently plucked and the LWC estimated using the oven drying method. The hand-held spectroradiometer and associated LWC data were then used to identify the pure-pixel narrowband normalised indices sensitive to LWC. The bands involved in the LWC indices were chosen based on their response to different water vibrational absorption regions of the electromagnetic spectrum. These indices were then calculated using the farm-scale hyperspectral images collected using the drone, and the minimum/maximum values of these indices and respective LWC used to generate synthetic data for training a gradient boosting machine (GBM) model. The GBM model was then evaluated on the actual farm data. The framework of this research is shown in Fig. 2.

### 2.1. Site description and data acquisition

The study was carried out during the post-monsoon season (*Rabi*) in a semi-arid area of Hyderabad, Telangana, India (17°19′27.2″N – 17°19′28.3″N and 78°23′55.4″E – 78°23′56.2″E). The farm location is shown in Fig. 3(a), being in the semi-arid zone with an average annual rainfall of 822 mm and annual potential evapotranspiration between 1700 and 1960 mm. The area has light red sandy-loam soil with around one meter of soil depth and bedrock beneath it. Maize crop (Zea mays L.) of variety 'Cargil 900 m gold' was selected for the research. The farm was maintained by Agricultural Research Institute, Professor Jayashankar Telangana State Agricultural University, Hyderabad, Telangana, India. The crop was sown during 2018–19 *Rabi* season (Post monsoon), with data collection during all growth stages of the crop growth. The experiment was laid out in split-plot design with a combination of three irrigation schedules and three fertilisation levels based on a climatological approach (Halagalimath, 2017). The ratio of irrigation water (IW) and cumulative pan evaporation (CPE) was used to decide the day on which plots need to be irrigated. Irrigation at IW/CPE

**Table 3**
Data collected from the research farm and their respective uses in this research.

| Data | Instrument used | Number of samples per plot/pixel size | Use of the data |
|---|---|---|---|
| Hyperspectral signatures | Spectroradiometer (SVC GER1500) (400–1000 nm) | Three signatures per leaf sample | Indices creation |
| High spatial and temporal resolution top-of-the-canopy hyperspectral images | Hexacopter-mounted Bayspec Hyperspectral imager (400–1000 nm) | Spatial resolution ~ 2 cm<br>Spectral resolution = 2.4 nm | Model training and testing |
| Leaf water content | 60–72 hour in an oven at 60 °C | One leaf per plot | Ground-truthing the leaf water estimation model |

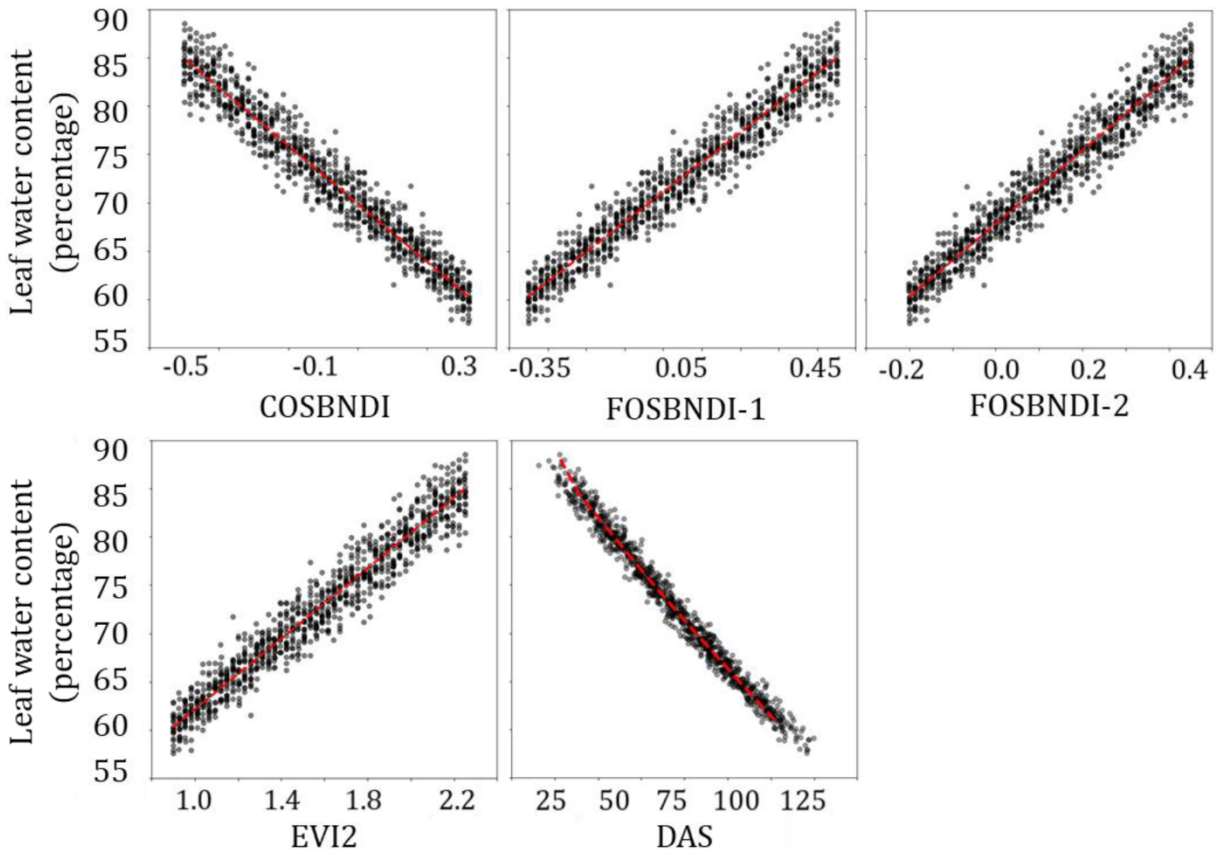


**Fig. 6.** Synthetic Leaf water content (LWC) data for the newly created indices and 'days after sowing' (DAS) information. The dashed red lines represent the interpolated values between the minimum and maximum of the index and LWC. The black dots represent Gaussian distributed points. The dashed line in the DAS-LWC plot represents a second-order polynomial fit line. (For interpretation of the references to color in this figure legend, the reader is referred to the web version of this article.)

ratio of 0.6, 0.8, and 1 was selected for plots with three irrigation levels. During each irrigation, 50 mm water was supplied to the scheduled plots through pipes directed through a water meter. Accordingly, IW was kept constant (50 mm) and daily readings from pan evaporimeters (in mm) used to find the IW/CPE ratio and thus timing of irrigation for the different plots. Three levels of nitrogen fertilisation (100, 200, and 300 kg nitrogen $ha^{-1}$) were given to each irrigation plot type. This combination of three irrigation and three fertilisation levels resulted in nine unique plots, and so with each replicated thrice, there was a total of 27 subplots (3 water × 3 nitrogen × 3 replications), as shown in Fig. 3(b). Each plot of size 4.2 m × 4.8 m was treated with one of the three different water and nitrogen levels to enable the subplots to be at low, medium and high water and fertiliser stress conditions. For each treatment, a plant to plant spacing of 20 cm and row to row spacing of 60 cm was adopted, resulting in a plant density of ~ 8.33 plants per $m^2$. Nitrogen was applied to all the plots at three different stages – sowing, six-leaf stage, and tasseling stage. Table 2 shows the various treatments used to create the plots drone-based top-of-canopy push-broom hyperspectral camera (Bayspec OCI-F-HR hyperspectral imager) was used to collect top-of-canopy farm images in the 400–1000 nm spectral range. The data were captured temporally from a height of 50 m above the ground having around 1 cm spatial resolution. The created hyperspectral cube of the farm map is shown in Fig. 4. After collection of hyperspectral images, a hand-held spectroradiometer of make Spectra Vista GER 1500 was used to collect leaf spectral signatures from one leaf of each of the 27 subplots. Three spectroradiometer readings were acquired from each leaf, and the leaf plucked and packed in an airtight pre-weighed zip bag for measuring the LWC. Fig. 5 shows the process of spectroradiometer data collection and LWC measurement. Table 3 shows the types of data collected from the farm.

### 2.2. Index selection for leaf water content

The number of bands in the spectroradiometer and hyperspectral imager data was 381 and 242, respectively. However, most of the bands in narrowband hyperspectral data show a high correlation to each other and thus contain similar information (Thenkabail and Lyon 2016). The

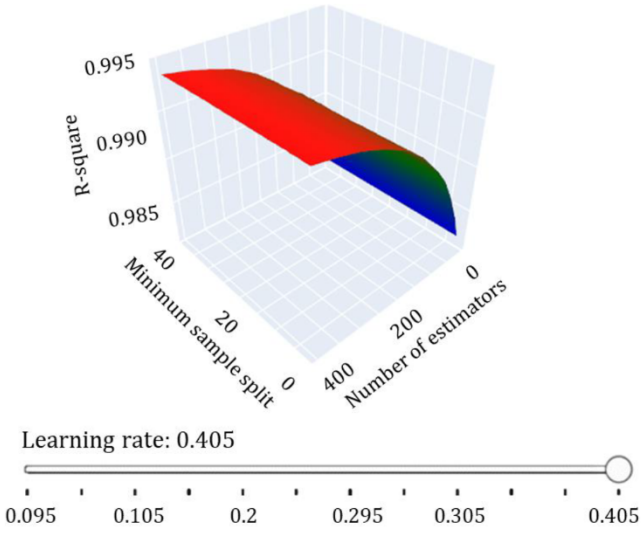


**Fig. 7.** Hyperparameter tuning graph for the Gradient Boosting Machine (GBM) algorithm. The best set of parameters was obtained at learning rate – 0.405, minimum sample split – 7, and the number of estimators – 400.

bands having redundant information or not having any relation with LWC should therefore be removed from the analysis as they create unnecessary complexity (Thenkabail and Lyon 2016). Thus, it is crucial to select only those bands which contain information about the LWC. One such approach of dimensionality reduction can be to choose only one band from the highly correlated set of bands. However, this band correlation method may discard the highly correlated bands having critical information about the crop parameter being measured (Kumar et al., 2001). Accordingly, Partial Least Square Regression has been used as a popular algorithm in chemometrics to reduce dimensionality, but this approach may not distinguish bands having little effect on the LWC (Hanrahan and Patil, 2005). Moreover, these models remain completely empirical in nature. It, therefore, becomes imperative to identify important bands for estimation of a specific crop property based on the science behind the electromagnetic spectrum's reflectance properties.

In this research, spectroradiometer data was used for identification of bands/indices for estimation of leaf water content. From 381 bands of spectroradiometer data ranging from 400 to 1000 nm, a total of 72,390 possible unique normalised difference indices were created according to

$$Normalised\ \ difference\ \ index\ \ (NDI) = \frac{Reflectance\ \ at\ \ band\ \ i - Reflectance\ \ at\ \ band\ \ j}{Reflectance\ \ at\ \ band\ \ i + Reflectance\ \ at\ \ band\ \ j} \quad (1)$$

where *i* and *j* are bands ranging from 400 to 1000 nm. Each of the indices was correlated with the actual leaf water content (measured after oven drying the leaves). The correlation heatmap is discussed in the results section. The highly correlated zones of the indices-LWC correlation heatmap were analysed with respect to the water-sensitive bands present in the 400–1000 nm wavelength region as discussed in the introduction section and in Table 1 towards LWC with drone-based hyperspectral data and only worked well with spectroradiometer data, limiting use of the later four indices in drone-based sensing applications.

### 2.3. Leaf water content estimation model

Based on the three newly identified indices (FOSBNDI-1, FOSBNDI-2 and COSBNDI), and the second version of Enhanced Vegetation Index (EVI2), farm index-maps were created using the drone-based hyperspectral data. EVI2 was selected due to its proven capability of being sensitive to equivalent water thickness of the canopy (Cheng et al., 2006, 2008), and calculated according to (Jiang et al., 2008)

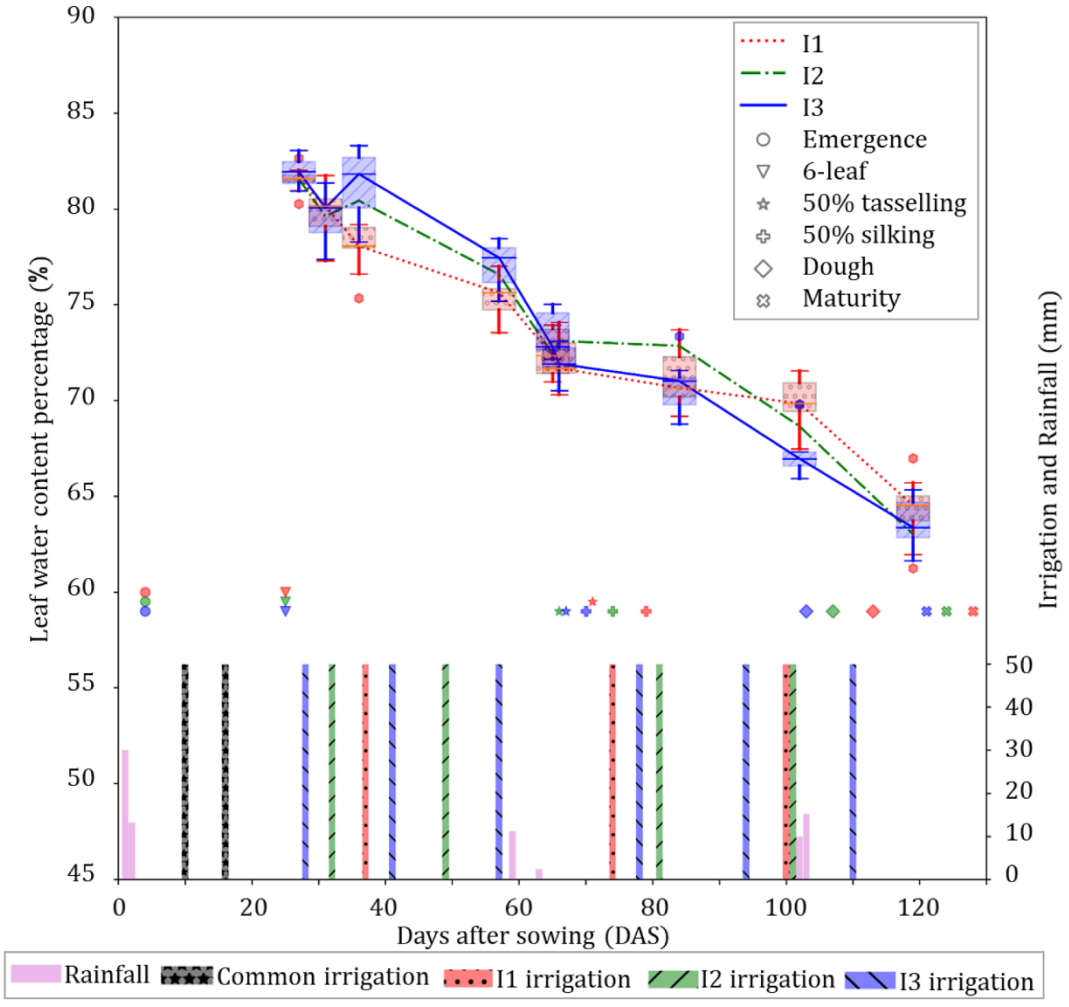


**Fig. 8.** Box-whisker plot of temporal leaf water content. I1, I2, and I3 are low, moderate, and no water stress treatment conditions, respectively. The secondary y-axis shows the irrigation and rainfall information.

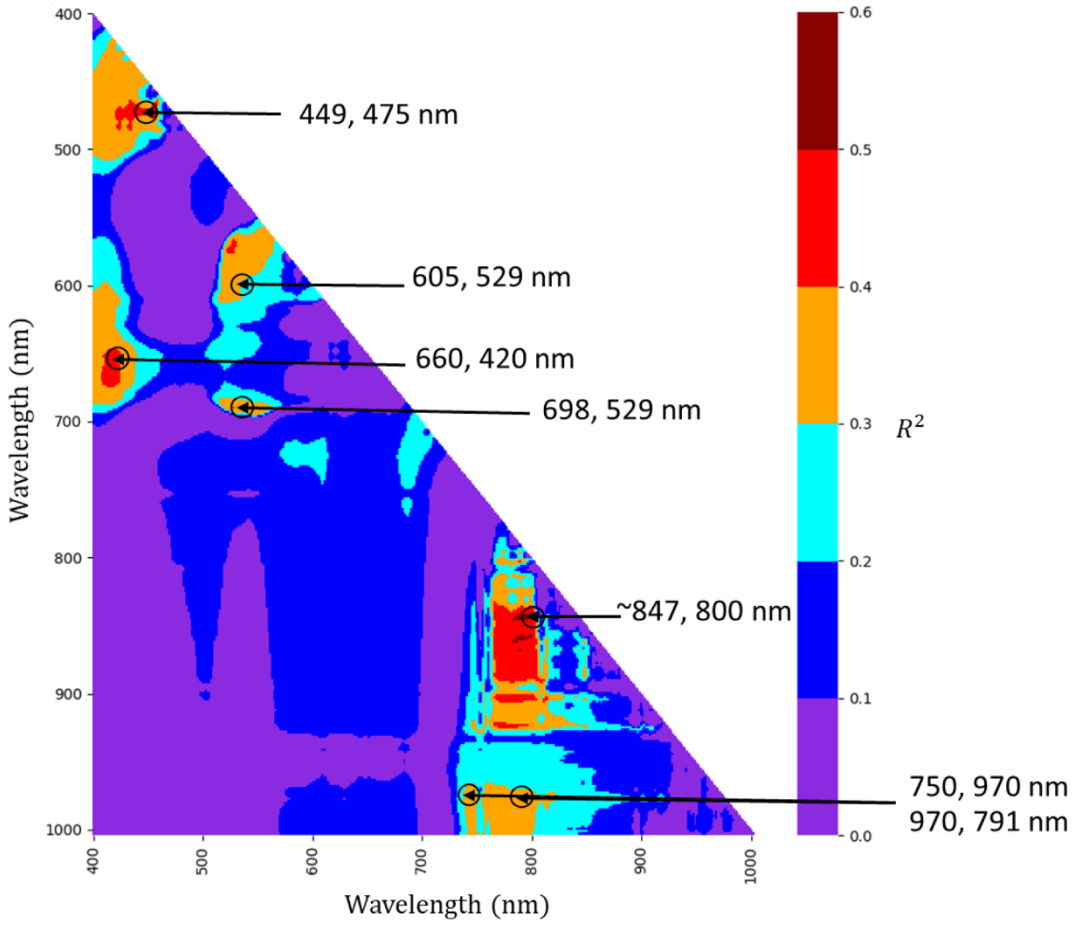


**Fig. 9.** Heatmap of the coefficient of determination between narrowband (two nm bandwidth) normalised difference vegetation indices and leaf-water content. The highly correlated indices are shown in brown/red colour, and least correlation indices are shown in violet colour. The indices created used the wavelengths shown on the × and y-axis as per Eq. (1). (For interpretation of the references to color in this figure legend, the reader is referred to the web version of this article.)

$$EVI2 = 2.5\left(\frac{NIR - R}{NIR + (6{*}R) - (7.5{*}B) + 1}\right) \quad (2)$$

As the images' spatial resolution was 1 cm, most of the vegetation pixels were scanned as pure pixels. However, to remove the background pixels (non-vegetation pixels) from the farm index maps, narrowband NDVI values of all the pixels were thresholded at a value of 0.7 and assigned a null value. These pixels included mostly non-vegetation pixels and some mixed pixels at the edges of the field.

The maximum and minimum value of each index-map of pure pixels was then used to generate synthetic data for model training as follows. Depending on the index and LWC relation (whether positively or negatively correlated), extreme index values were assigned to the highest and lowest LWC values, respectively. Assuming a linear relationship, a straight line was interpolated between the extreme values of the indices and LWC, as shown by the dashed line in Fig. 6. The linear relation was chosen as it has no spectral saturation (Tian et al., 2011), and Pasqualotto et al. (2018) and Sun et al. (2019) have found that a linear relation with LWC gives a better estimation than exponential or polynomial relations. Considering the interpolated values as being the mean of an observational distribution for LWC, 1,000 Gaussian

**Table 4**
Vegetation pure pixel, narrowband indices for estimation of leaf water content.

| Index Formula | short from | Full form | Range | Usability |
|---|---|---|---|---|
| $\frac{R660 - R420}{R660 + R420}$ | COSBNDI | Combined overtone of stretching bands - normalised difference index | −0.50 to 0.30 (Negative correlation) | Spectroradiometer and drone data |
| $\frac{R529 - R698}{R529 + R698}$ | FOSBNDI-1 | Forth overtone of stretching bands - normalised difference index 1 | −0.35 to 0.45 (Postive correlation) | |
| $\frac{R529 - R605}{R529 + R605}$ | FOSBNDI-2 | Forth overtone of stretching bands - normalised difference index 2 | −0.20 to 0.45 (Positive correlation) | |
| $\frac{R475 - R449}{R475 + R449}$ | FSOSBNDI | Fifth and sixth overtone of stretching bands - normalised difference index | −0.20 to 0.45 (Negative correlation) | Spectroradiometer data only |
| $\frac{R750 - R970}{R750 + R970}$ | SAPSBNDI | Small absorption peak of stretching bands - normalised difference index | −0.27 to 0.68 (Positive correlation) | |
| $\frac{R791 - R970}{R791 + R970}$ | SOSBNDI | Second overtone of stretching bands - normalised difference index | ~-0.15 to 0.65 (Positive correlation) | |
| $\frac{R800 - R847}{R800 + R847}$ | WASCOSBNDI | Water absorption shoulder due to combined overtone of stretching bands - normalised difference index | ~0 to 0.2 (Positive correlation) | |

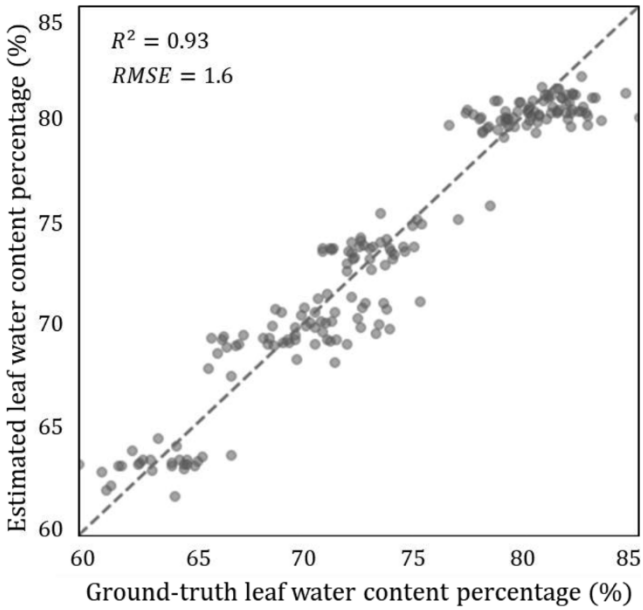


**Fig. 10.** Evaluation of the GBM model trained on the synthetic data against spectroradiometer data. The dots of the scatterplot are semi-transparent. Relatively darker areas of the scatterplot shows overlapping of points in those regions.

distributed points were generated within 10% of the interpolated LWC value. The generated points are shown by the black dots in Fig. 6. Along with this index-LWC synthetic data, crop growth-stage based LWC synthetic data was also created. Here a second-order polynomial fit line was selected as it gave a better representation of the temporal LWC, with a Gaussian noise generated within 5% of the interpolated LWC values.

A total of 20,000 sets of points were used from the synthetic data to train the GBM model developed to estimate LWC. The GBM was selected as it combines the predictions from multiple decision trees to generate a final prediction. The GBM performs the sequential improvement of decision trees to convert weak learners into strong learners, and produce the best metrics for the algorithm to fit the data by tuning the hyperparameters (Friedman, 2001). The hyperparameters of the GBM regression were tuned, and the optimal values selected for model's weights. The hyperparameter tuning result is shown in Fig. 7. The model trained on synthetic data was then implemented on the index maps obtained from the drone-based hyperspectral data.

## 3. Results

The temporal details of irrigation, rainfall, LWC, and growth stages are shown in Fig. 8. The various treatments provided in the subplots resulted in different water content of the plant leaves. The general nature of decreasing LWC means that the water percentage in a leaf per unit fresh leaf weight (Ma et al., 2018) reduces as the crop moves towards maturity. Another critical observation of Fig. 8 is that the LWC in the I3 irrigated plots were higher than I1 irrigated plots until the tasselling stage. After the tasselling stage, the I3 irrigated plants showed lower LWC than the I1 irrigated plants. This occurred due to delayed growth stage in the I1 irrigated crops. The I3 irrigated plants showed higher LWC than I1 irrigated plants during the crop's vegetative stage. Tasseling, silking, dough, and maturity stages were found to be delayed for I1 irrigated plants when compared to I3 irrigated plants. It was also seen that until 28 DAS, when all the plots were irrigated uniformly, the LWC was also in the same range for all the plots. On 28 DAS, when only the I3 plots were irrigated, the LWC was seen to be higher in I3 than I1. Rainfall around 60 DAS made the LWC in the same range for all the plots. These temporal variations in LWC show the capability of detecting instantaneous water stress in a maize crop using LWC information.

The LWC correlation heatmap created using 72,390 unique indices as explained in Eq. (1) is shown in Fig. 9. Analysis of the correlation heatmap clearly showed that the wavelengths associated with water absorption bands created the highest correlation regions. Thus, index selection was made based on those indices that gave the highest correlation when coupled with the water absorption bands. Fig. 9 shows the heatmap with marked water absorption wavelengths. The indices created using brown/red zone wavelengths showed maximum correlation, while the indices created using the violet zone showed the least correlation with maize LWC. The identified indices are shown in Table 4.

The GBM model created in this research was evaluated on spectroradiometer based index data with an $R^2$ of 0.93 and RMSE of 1.6% (g/g), as shown in Fig. 10. The GBM model was also evaluated for the 6-leaf stage (35 DAS) and late-vegetative stage (56 DAS) farm maps. Fig. 11 shows the colour-coded farm maps for better visualisation of the spatial distribution of LWC in the farm. The map visualisation methods explained in Crameri et al. (2020) have been used to create the color coded LWC maps of the farm. Accordingly, the farm-map has been

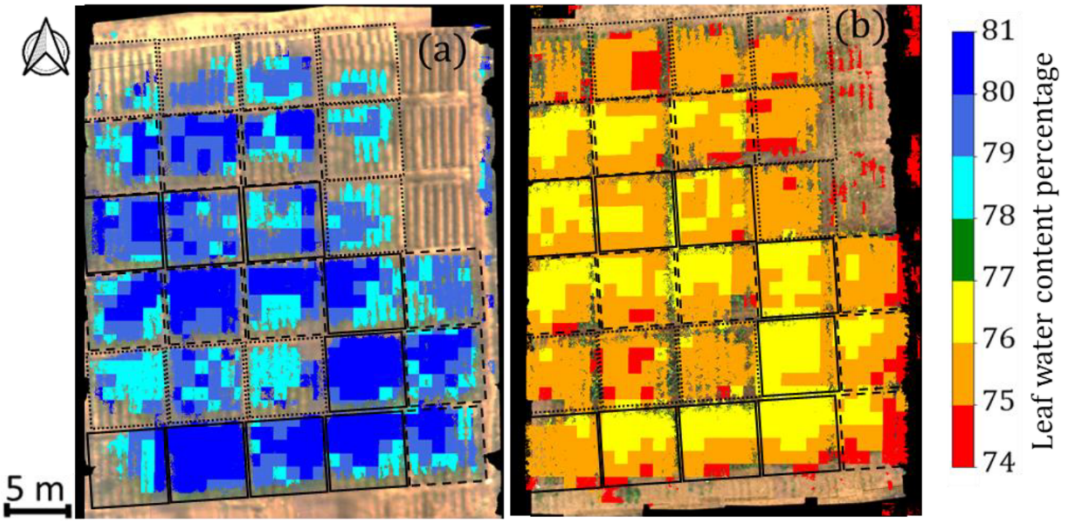


**Fig. 11.** Colour coded leaf water content (LWC) maps of a maize farm. (a) The LWC farm map at the 6-leaf stage (35 days after sowing); (b) The LWC farm map at late-vegetative stage (56 days after sowing). The LWC difference of well irrigated (solid line boxes with I3 irrigation), moderately irrigated (dashed line boxes) and less irrigated (dotted line boxes) plots can be easily seen in the farm maps.

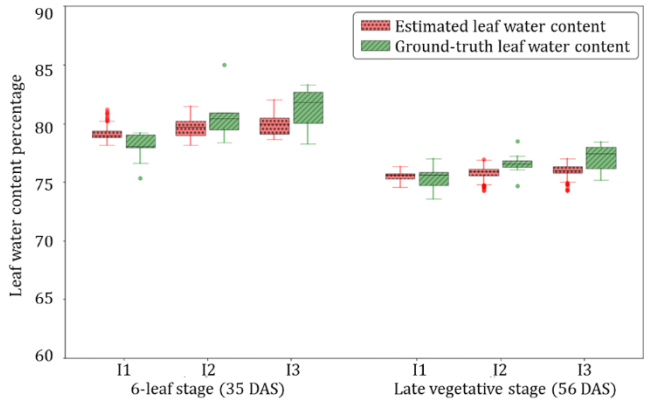


**Fig. 12.** Box-whisker plots of estimated and ground-truth leaf water content for the 6-leaf stage and late vegetative stage plants. The 6-leaf stage data were collected at 35 days after sowing (DAS) and the late vegetative stage data were collected at 56 DAS. I1, I2, and I3 represent the three irrigation levels applied in the different plots of the research farm, with I3 representing sufficient irrigation, I2 moderate, and I1 water-stressed plots.

smoothed with a gaussian filter and overlayed with different line-type boxes to indicate the I1, I2, and I3 irrigation plots. For the 6-leaf and late-vegetative stage maps, water-stressed plots (I1) could easily be identified as having lower LWC. This can be verified from the box-whisker plot shown in Fig. 8, where the 35 and 56 DAS plant's LWC of I1 plot were less than that for the I3 plot plants. However, the visual difference between I2 and I3 plots cannot be seen. The box-whisker plots of different irrigation treatment plots and ground truth data are shown in Fig. 12.

## 4. Discussion

The water absorption indices and LWC model developed in this research can be used for early growth stage (from 6-leaf stage to tasselling stage) leaf water content estimation of a crop using narrowband pure pixel airborne optical data. Indices were developed using handheld spectroradiometer data taken from approximately 10 cm distance from leaves and applied to drone-based data obtained from about 50 m distance from the leaves, with three of the seven indices found to show the sensitivity needed for LWC estimation of crops treated with different irrigation amounts. This highlights the utility of the three indices (FOSBNDI-1, FOSBNDI-2, and COSBNDI) in the field of drone-based sensing. However, as these indices have been derived from pure vegetation pixel data, implementation of these indices on mixed pixel data may drastically reduce the sensitivity to LWC. Importantly, with the distance between the leaves and the drone-based sensor being only 50 m, the atmospheric effect on the hyperspectral data is minimal compared to that on satellite or airborne data. However, the other four LWC indices identified from the spectroradiometer (FSOSBNDI, SAPBNDI, SOSBNDI, and WASCOSBNDI) may still have lost their sensitivity when applied to UAV data due to the increased distance between the leaf and sensor. Importantly, by training the model to synthetic data, the model will have a reduced dependence on the collected data, meaning that it should be applicable to other fields and seasons with the same maize variety.

Another interesting observation is that these indices lose sensitivity

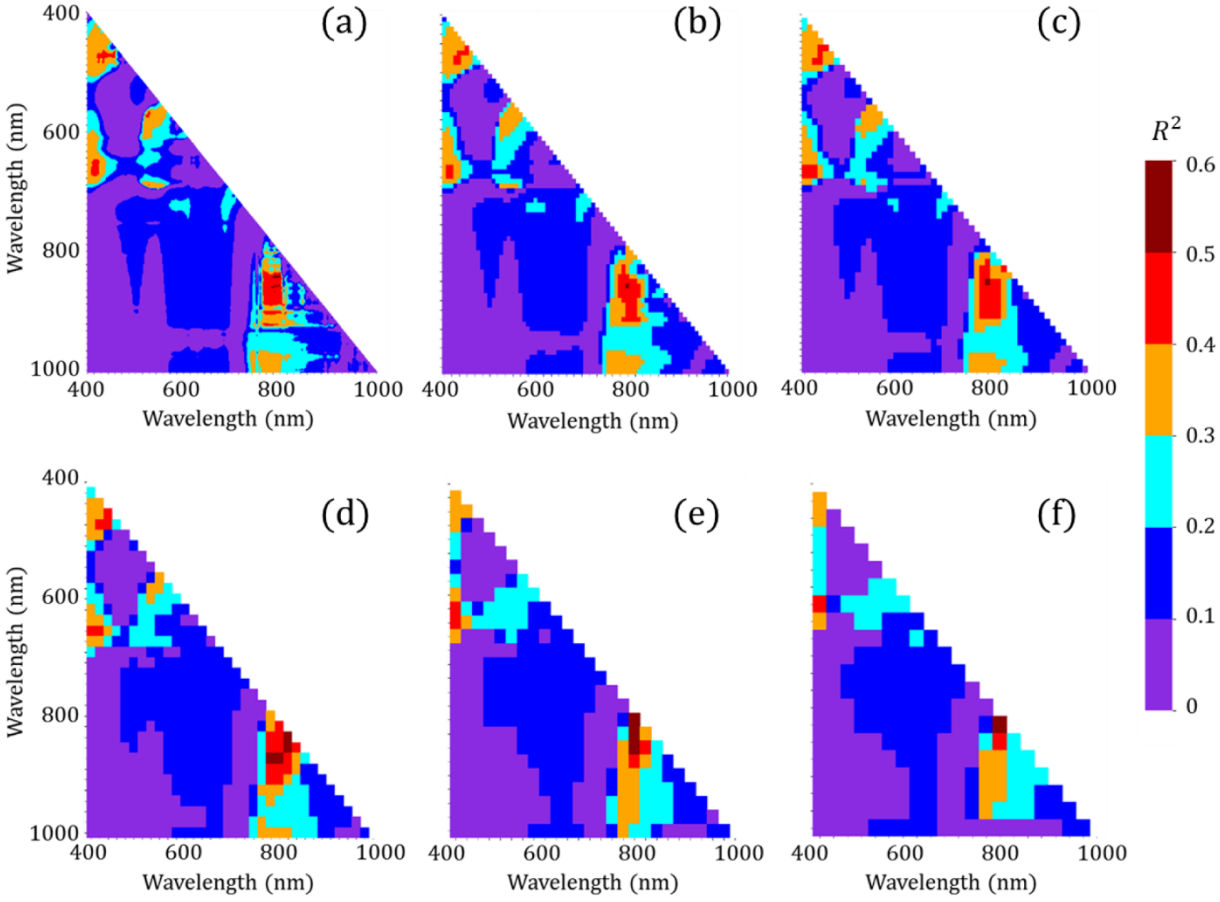


**Fig. 13.** Comparison of heatmaps of the coefficient of determination between normalised difference vegetation indices of different bandwidth and leaf-water content. The bandwidths used to create these heatmaps are as follows: (a) 2 nm, (b) 8 nm, (c) 11 nm, (d) 18 nm, (e) 22 nm, and (f) 30 nm. The indices created used the wavelengths shown on the x and y-axis as per Eq. (1).

as the bandwidth is increased. The analysis was done on different bandwidth data (2 nm to 30 nm) by creating multiple index-LWC correlation heatmap. The correlation heatmap comparison is given in Fig. 13. A correlation similar to the 2 nm bandwidth indices is observed until 11 nm bandwidth, after which there is substantially less sensitivity towards LWC. Thus, this research suggests that for LWC estimation, sensors should be made by considering the wavelengths given in Table 4 as central wavelength with less than 11 nm bandwidth for each band. Moreover, researchers from different parts of the world should use and test the indices/wavelengths presented in Table 1 and Table 4 on various crops to estimate LWC.

There are multiple studies which have used hyperspectral data to estimate the leaf/vegetation water content. However, most of them have acquired data from the entire 400–2500 nm range to utilise the primary water absorption bands. Moreover, process-based models like PROSPECT/ PROSAIL do not produce any change in the 400–900 nm spectra when LWC changes in the crop. Pasqualotto et al. (2018) have used airborne 400–2500 nm data to get the canopy water content for multiple crop types (lucerne, corn, potato, sugar beet and onion). The authors have used primary water absorption bands to get water absorption area and depth water index. Using these indices with an exponential fit, the authors achieved an $R^2$ of around 0.75, but the model could not perform well for areas having less than 30% of vegetation cover. Herrmann et al. (2020) used an 11 band drone-based hyperspectral imager to collect temporal data from a maize crop. The study identified 570 nm and 620 nm wavelengths as being more sensitive to different irrigation crop treatments. The study also estimated relative crop water content using a partial least square regression on all 11 bands (420, 440, 490, 550, 640, 670, 700, 740, 780, 860 and 910 nm) with an $R^2$ of 0.55.

In another study, Sun et al., (2019) used spectroradiometer data in the range 400–2500 nm to estimate LWC of a winter wheat crop. Various indices were tested and an $R^2$ of 0.77 achieved. Cheng et al. (2011) used 350–2500 nm spectroscopic data to estimate the LWC of 47 species present in the tropical forests of Panama using continuous wavelet analysis. The model had an $R^2$ in the range of 0.71–0.75. In contrast, Corti et al., (2017) used 400–1000 nm hyperspectral imager data to estimate spinach canopy water content using a partial least square regression model and achieved an $R^2$ of 0.87. By comparison, the research presented in this paper achieved an $R^2$ of 0.93 and RMSE of 1.6% (g/g) even when applied exclusively to early vegetative stages of the maize crop. This shows that the 400–1000 nm sensors' cost-effectiveness and usefulness of identified optimal bands make this range equally powerful for pure-pixel data as compared to 400–2500 nm data. Moreover, the sensors that capture data in the range of 400–2500 nm are costly and give enormous data volumes, which also creates storage and analysis issues.

## 5. Conclusion

This research has developed a new approach for leaf water content (LWC) estimation at an early crop growth stage using hyperspectral data from only the 400–1000 nm range. Seven indices were created using spectroradiometer data based on the overtone frequencies of O-H bonds of water molecules. Three of the seven indices were shown to have sensitivity for LWC estimation from drone-based hyperspectral data. The model created from these indices has shown precise estimation of LWC at the 6-leaf stage and before tasselling stage of the crop growth with an $R^2$ of 0.93 and RMSE of 1.6% (g/g). This early growth stage LWC estimation can be used to identify water-stressed plots and thus potential yield loss can be avoided. Accordingly, this model can be used for estimating spatial and temporal LWC changes across farms in near real-time to undertake decision making on irrigation management.

## Declaration of Competing Interest

The authors declare that they have no known competing financial interests or personal relationships that could have appeared to influence the work reported in this paper.

*Acknowledgement*

The authors would like to acknowledge BharatRohan company for their help in flying the drone for data collection and Professor Jayashankar Telangana State Agricultural University for providing the farm test-bed for carrying out the research. The critical reviews and suggestions during project progress presentations from all the members of the DST-JST project has refined this study and helped in achieving better results.

*Funding*

This research was jointly funded by the Department of Science and Technology (DST); Ministry of Science and Technology, Government of India; and Japan Science and Technology (JST), Government of Japan (DST/INT/JST/P-29/2016). IITB-Monash Research Academy has funded the resources used in the research.

## References

Abowarda, A.S., Bai, L., Zhang, C., Long, D., Li, X., Huang, Q., Sun, Z., 2021. Generating surface soil moisture at 30 m spatial resolution using both data fusion and machine learning toward better water resources management at the field scale. Remote Sens. Environ. 255, 112301.

Aroca, R., 2012. Plant responses to drought stress. In: From morphological to molecular features. Springer-Verlag, Berlin Heidelberg, pp. 1–5.

Blum, A., 2011. Plant water relations, plant stress and plant production. In: In Plant breeding for water-limited environments. Springer, New York, NY, pp. 11–52.

Braun, G.L., Smirnov, S.N., 1993. Why is water blue? J. Chem. Educ. 70 (8), 612.

Büning-Pfaue, H., 2003. Analysis of water in food by near infrared spectroscopy. Food Chem. 82 (1), 107–115.

Crameri, F., Shephard, G.E., Heron, P.J., 2020. The misuse of colour in science communication. Nat. Commun. 11 (1), 1–10.

Carter, G.A., 1991. Primary and secondary effects of water content on the spectral reflectance of leaves. Am. J. Bot. 78 (7), 916–924.

Casas, A., Riaño, D., Ustin, S.L., Dennison, P., Salas, J., 2014. Estimation of water-related biochemical and biophysical vegetation properties using multitemporal airborne hyperspectral data and its comparison to MODIS spectral response. Remote Sens. Environ. 148, 28–41.

Ceccato, P., Flasse, S., Tarantola, S., Jacquemoud, S., Grégoire, J.M., 2001. Detecting vegetation leaf water content using reflectance in the optical domain. Remote Sens. Environ. 77 (1), 22–33.

Clevers, J.G., Kooistra, L., Schaepman, M.E., 2010. Estimating canopy water content using hyperspectral remote sensing data. Int. J. Appl. Earth Obs. Geoinf. 12 (2), 119–125.

Chaplin, M., 2008. Water absorption spectrum. Water Structure and Science.

Chen, D., Huang, J., Jackson, T.J., 2005. Vegetation water content estimation for corn and soybeans using spectral indices derived from MODIS near-and short-wave infrared bands. Remote Sens. Environ. 98 (2–3), 225–236.

Cheng, T., Rivard, B., Sanchez-Azofeifa, A., 2011. Spectroscopic determination of leaf water content using continuous wavelet analysis. Remote Sens. Environ. 115 (2), 659–670.

Cheng, Y.B., Zarco-Tejada, P.J., Riaño, D., Rueda, C.A., Ustin, S.L., 2006. Estimating vegetation water content with hyperspectral data for different canopy scenarios: Relationships between AVIRIS and MODIS indexes. Remote Sens. Environ. 105 (4), 354–366.

Cheng, Y.B., Ustin, S.L., Riaño, D., Vanderbilt, V.C., 2008. Water content estimation from hyperspectral images and MODIS indexes in Southeastern Arizona. Remote Sens. Environ. 112 (2), 363–374.

Corti, M., Gallina, P.M., Cavalli, D., Cabassi, G., 2017. Hyperspectral imaging of spinach canopy under combined water and nitrogen stress to estimate biomass, water, and nitrogen content. Biosyst. Eng. 158, 38–50.

Etminan, A., Tabatabaeenejad, A., Moghaddam, M., 2020. Retrieving Root-Zone Soil Moisture Profile From P-Band Radar via Hybrid Global and Local Optimization. IEEE Trans. Geosci. Remote Sens. 58 (8), 5400–5408.

Fan, W., Hu, B., Miller, J., Li, M., 2009. Comparative study between a new nonlinear model and common linear model for analysing laboratory simulated-forest hyperspectral data. Int. J. Remote Sens. 30 (11), 2951–2962.

Feilhauer, H., Asner, G.P., Martin, R.E., 2015. Multi-method ensemble selection of spectral bands related to leaf biochemistry. Remote Sens. Environ. 164, 57–65.

Finn, M.P., Lewis, M., Bosch, D.D., Giraldo, M., Yamamoto, K., Sullivan, D.G., Kincaid, R., Luna, R., Allam, G.K., Kvien, C., Williams, M.S., 2011. Remote sensing of soil moisture using airborne hyperspectral data. GIScience Remote Sens. 48 (4), 522–540.

Friedman, J.H., 2001. Greedy function approximation: a gradient boosting machine. Ann. Stat. 1189–1232.

Gabriel, J.L., Zarco-Tejada, P.J., Juan López-Herrera, P., Pérez-Martín, Enrique, Alonso-Ayuso, Maria, Quemada, Miguel, 2017. Airborne and Ground Level Sensors for Monitoring Nitrogen Status in a Maize Crop. Biosyst. Eng. 160, 124–133.

G. Hanrahan, F. Udeh, D.G. Patil, Chemometrics and Statistics | Multivariate Calibration Techniques, Editor(s): Paul Worsfold, Alan Townshend, Colin Poole,Encyclopedia of Analytical Science (Second Edition), Elsevier, 2005, Pages 27-32, ISBN 9780123693976.

Gao, B.C., Montes, M.J., Davis, C.O., Goetz, A.F., 2009. Atmospheric correction algorithms for hyperspectral remote sensing data of land and ocean. Remote Sens. Environ. 113, S17–S24.

Gao, Y., Walker, J.P., Allahmoradi, M., Monerris, A., Ryu, D., Jackson, T.J., 2015. Optical sensing of vegetation water content: a synthesis study. IEEE J. Sel. Top. Appl. Earth Obs. Remote Sens. 8 (4), 1456–1464.

Gonzalez-Dugo, V., Durand, J.L., Gastal, F., 2010. Water deficit and nitrogen nutrition of crops. A review. Agronomy Sustain. Develop. 30 (3), 529–544.

Hadjimitsis, D.G., Clayton, C.R.I., Hope, V.S., 2004. An assessment of the effectiveness of atmospheric correction algorithms through the remote sensing of some reservoirs. Int. J. Remote Sens. 25 (18), 3651–3674.

Halagalimath, S.P., 2017. Effect of scheduling irrigation and mulching on growth and yield of maize (Zea mays L.). J. Farm Sci. 30 (1), 45–48.

Han, M., Zhang, H., DeJonge, K.C., Comas, L.H., Trout, T.J., 2016. Estimating maize water stress by standard deviation of canopy temperature in thermal imagery. Agric. Water Manag. 177, 400–409.

Herrmann, I., Bdolach, E., Montekyo, Y., Rachmilevitch, S., Townsend, P.A., Karnieli, A., 2020. Assessment of maize yield and phenology by drone-mounted superspectral camera. Precis. Agric. 21 (1), 51–76.

Hsiao, T.C., 1973. Plant responses to water stress. Annu. Rev. Plant Physiol. 24 (1), 519–570.

Hsiao, T.C., Fereres, E., Acevedo, E., Henderson, D.W., 1976. Water stress and dynamics of growth and yield of crop plants. In: Water and plant life. Springer, Berlin, Heidelberg, pp. 281–305.

Huang, Y., Walker, J.P., Gao, Y., Wu, X., Monerris, A., 2015. Estimation of vegetation water content from the radar vegetation index at L-band. IEEE Trans. Geosci. Remote Sens. 54 (2), 981–989.

Hunt Jr, E.R., Li, L., Yilmaz, M.T., Jackson, T.J., 2011. Comparison of vegetation water contents derived from shortwave-infrared and passive-microwave sensors over central Iowa. Remote Sens. Environ. 115 (9), 2376–2383.

Hunter, K.M., Shakib, F.A., Paesani, F., 2018. Disentangling coupling effects in the infrared spectra of liquid water. J. Phys. Chem. B 122 (47), 10754–10761.

Jiang, Z., Huete, A.R., Didan, K., Miura, T., 2008. Development of a two-band enhanced vegetation index without a blue band. Remote Sens. Environ. 112 (10), 3833–3845.

Jones, H.G., Sirault, X.R., 2014. Scaling of thermal images at different spatial resolution: the mixed pixel problem. Agronomy 4 (3), 380–396.

Kim, Y., Glenn, D.M., Park, J., Ngugi, H.K., Lehman, B.L., 2010. In: Hyperspectral image analysis for plant stress detection. American Society of Agricultural and Biological Engineers, p. (p. 1)..

Kim, Y., Still, C.J., Hanson, C.V., Kwon, H., Greer, B.T., Law, B.E., 2016. Canopy skin temperature variations in relation to climate, soil temperature, and carbon flux at a ponderosa pine forest in central Oregon. Agric. For. Meteorol. 226, 161–173.

Kokaly, R.F., Clark, R.N., 1999. Spectroscopic determination of leaf biochemistry using band-depth analysis of absorption features and stepwise multiple linear regression. Remote Sens. Environ. 67 (3), 267–287.

Kumar, S., Ghosh, J., Crawford, M.M., 2001. Best-bases feature extraction algorithms for classification of hyperspectral data. IEEE Trans. Geosci. Remote Sens. 39 (7), 1368–1379.

Ma, X., He, Q., Zhou, G., 2018. Sequence of Changes in Maize Responding to Soil Water Deficit and Related Critical Thresholds. Front. Plant Sci. 9, 511.

Merlin, O., Al Bitar, A., Walker, J.P., Kerr, Y., 2010. An improved algorithm for disaggregating microwave-derived soil moisture based on red, near-infrared and thermal-infrared data. Remote Sens. Environ. 114 (10), 2305–2316.

Mohorič, T., Bren, U., 2020. How does microwave irradiation affect the mechanism of water reorientation? J. Mol. Liq. 302, 112522.

Mueller, N.D., Gerber, J.S., Johnston, Matt, Ray, D.K., Ramankutty, Navin, Foley, J.A., 2012. Closing Yield Gaps through Nutrient and Water Management. Nature 490 (7419), 254–257.

Neinavaz, E., Skidmore, A.K., Darvishzadeh, R., Groen, T.A., 2017. Retrieving vegetation canopy water content from hyperspectral thermal measurements. Agric. For. Meteorol. 247, 365–375.

Pasqualotto, N., Delegido, J., Van Wittenberghe, S., Verrelst, J., Rivera, J.P., Moreno, J., 2018. Retrieval of canopy water content of different crop types with two new hyperspectral indices: Water Absorption Area Index and Depth Water Index. Int. J. Appl. Earth Obs. Geoinf. 67, 69–78.

Pinheiro, C., Chaves, M.M., 2011. Photosynthesis and drought: can we make metabolic connections from available data? J. Exp. Bot. 62 (3), 869–882.

Pope, R.M., Fry, E.S., 1997. Absorption spectrum (380–700 nm) of pure water II. Integrating cavity measurements. Appl. Opt. 36, 8710–8723.

Thenkabail, P.S. and Lyon, J.G. eds., 2016. Hyperspectral remote sensing of vegetation. CRC press.

Reddy, T.Y., Reddy, V.R., Anbumozhi, V., 2003. Physiological responses of groundnut (Arachis hypogea L.) to drought stress and its amelioration: a critical review. Plant Growth Regul. 41 (1), 75–88.

Schulze, E.D., Hall, A.E., 1982. Stomatal responses, water loss and $CO_2$ assimilation rates of plants in contrasting environments. In: Physiological plant ecology II. Springer, Berlin, Heidelberg, pp. 181–230.

Shen, X., Walker, J.P., Ye, N., Wu, X., Boopathi, N., Yeo, I.Y., Zhang, L., Zhu, L., 2020. Soil Moisture Retrieval Depth of P-and L-Band Radiometry: Predictions and Observations. IEEE Transactions on Geoscience and Remote Sensing.

Sicard, M., Thome, K.J., Crowther, B.G., Smith, M.W., 1998. Shortwave infrared spectroradiometer for atmospheric transmittance measurements. J. Atmos. Oceanic Technol. 15 (1), 174–183.

Sogandares, F.M., Fry, E.S., 1997. Absorption spectrum (340–640 nm) of pure water I. Photothermal measurements. Appl. Opt. 33, 8699–8709.

Stomp, M., Huisman, J., Stal, L.J., Matthijs, H.C., 2007. Colorful niches of phototrophic microorganisms shaped by vibrations of the water molecule. ISME J. 1 (4), 271–282.

Sun, H., Feng, M., Xiao, L., Yang, W., Wang, C., Jia, X., Zhao, Y., Zhao, C., Muhammad, S. K., Li, D., 2019. Assessment of plant water status in winter wheat (Triticum aestivum L.) based on canopy spectral indices. PLoS ONE 14 (6), e0216890.

Tian, Y.C., Yao, X., Yang, J., Cao, W.X., Hannaway, D.B., Zhu, Y., 2011. Assessing newly developed and published vegetation indices for estimating rice leaf nitrogen concentration with ground-and space-based hyperspectral reflectance. Field Crops Res. 120 (2), 299–310.

Thenkabail, P.S., Smith, R.B., De Pauw, E., 2002. Evaluation of narrowband and broadband vegetation indices for determining optimal hyperspectral wavebands for agricultural crop characterization. Photogramm. Eng. Remote Sens. 68 (6), 607–622.

Thompson, D.R., Guanter, L., Berk, A., Gao, B.C., Richter, R., Schläpfer, D., Thome, K.J., 2019. Retrieval of atmospheric parameters and surface reflectance from visible and shortwave infrared imaging spectroscopy data. Surv. Geophys. 40 (3), 333–360.

Thorpe, M.J., Moll, K.D., Jones, R.J., Safdi, B., Ye, J., 2006. Broadband cavity ringdown spectroscopy for sensitive and rapid molecular detection. Science 311 (5767), 1595–1599.

Tsubomura, H., Yamamoto, N., Matsuo, N., Okada, Y., 1980. The visible absorption spectrum of water. Proc. Japan Acad. Series B 56 (7), 403–407.

Walker, J.P., Houser, P.R., Willgoose, G.R., 2004. Active microwave remote sensing for soil moisture measurement: a field evaluation using ERS-2. Hydrol. Process. 18 (11), 1975–1997.

Wang, X. and Xing, Y., 2016. Effects of irrigation and nitrogen fertilizer input levels on soil-n content and vertical distribution in greenhouse tomato (Lycopersicum esculentum Mill.). Scientifica, 2016.

Underwood, J., Wittig, C., 2004. Two-photon photodissociation of H2O via the B state. Chem. Phys. Lett. 386 (1–3), 190–195.

Vogelmann, T.C., 1993. Plant tissue optics. Annu. Rev. Plant Biol. 44 (1), 231–251.

Xu, C., Zeng, W., Huang, J., Wu, J., Van Leeuwen, W.J., 2016. Prediction of soil moisture content and soil salt concentration from hyperspectral laboratory and field data. Remote Sensing 8 (1), 42.

Yakovenko, A.A., Yashin, V.A., Kovalev, A.E., Fesenko, E.E., 2002. Structure of the vibrational absorption spectra of water in the visible region. Biophysics-Pergamon-C/C Biofizika 47 (6), 891–895.

Yilmaz, M.T., Hunt Jr, E.R., Jackson, T.J., 2008. Remote sensing of vegetation water content from equivalent water thickness using satellite imagery. Remote Sens. Environ. 112 (5), 2514–2522.

Zheng, W. and ZENG, Z.Y., 2004. A review on methods of atmospheric correction for remote sensing images. Remote Sensing Information, 4, pp.66-67.

Zygielbaum, A.I., Gitelson, A.A., Arkebauer, T.J., Rundquist, D.C., 2009. Non-destructive detection of water stress and estimation of relative water content in maize. Geophys. Res. Lett. 36 (12).